Removal of developmentally regulated microexons has a minimal impact on larval zebrafish brain morphology and function

Caleb C.S. Calhoun[1], Mary E.S. Capps[1,2], Kristie Muya[1], William C. Gannaway[1], Verdion Martina[1], Claire L. Conklin[1], Morgan C. Klein[1], Jhodi Webster[1], Emma G. Torija-Olson[1], Summer B. Thyme[1,2]*

1. Department of Neurobiology, The University of Alabama at Birmingham Heersink School of Medicine, Birmingham, AL, USA
2. Present Address: Department of Biochemistry and Molecular Biotechnology, UMass Chan Medical School, Worcester, MA, USA

* Correspondence may be addressed to Summer B. Thyme (Email: Summer.Thyme@umassmed.edu).

Abstract

Microexon splicing is a vertebrate-conserved process through which small, often in-frame, exons are differentially included during brain development and across neuron types. Although the protein sequences encoded by these exons are highly conserved and can mediate interactions, the neurobiological functions of only a small number have been characterized. To establish a more generalized understanding of their roles in brain development, we used CRISPR/Cas9 to remove 45 microexons in zebrafish and assessed larval brain activity, morphology, and behavior. Most mutants had minimal or no phenotypes at this developmental stage. Among previously studied microexons, we uncovered baseline and stimulus-driven phenotypes for two microexons (meA and meB) in *ptprd* and reduced activity in the telencephalon in the *tenm3* B_0 isoform. Although mild, neural phenotypes were discovered for several microexons that have not been previously characterized, including in *ppp6r3*, *sptan1*, *dop1a*, *rapgef2*, *dctn4*, *vti1a*, and *meaf6.* This study establishes a general approach for investigating conserved alternative splicing events and prioritizes microexons for downstream analysis.

Introduction

Alternative splicing greatly expands proteome diversity and can impact brain development and disease (Vuong et al., 2016). As most metazoan proteins are represented by multiple isoforms, defining the functional significance of individual splicing events is a vast challenge. Mouse studies do not have the throughput to assess the neural role of 10s or 100s of isoforms, and cell culture does not recapitulate the complex development of an animal brain.

One class of particularly conserved and developmentally regulated spliced exons is microexons or mini-exons. These small exons, 3-30 nucleotides or 1-10 amino acids in length, are either gained or lost in transcripts in the brain compared to other tissues. While most are in-frame, this pathway can also trigger nonsense-mediated decay to influence protein levels (Lin et al., 2020). Although these neuron-specific exons were recognized almost 40 years ago (Brugge et al., 1985; Martinez et al., 1987), their discovery and annotation have continued into recent years (Parada et al., 2021). Thus far, hundreds have been identified. Although more than one splicing regulator has been implicated in the alternative inclusion of microexons in neurons (Ciampi et al., 2022; Y. I. Li et al., 2015), many are controlled by the vertebrate-specific protein SRRM4 (Irimia et al.,

2014; Quesnel-Vallières et al., 2015). Srrm4 interacts with Srsf11 and Rnps1 at polypyrimidine sequences upstream of microexons to regulate their inclusion (Gonatopoulos-Pournatzis et al., 2018).

Proteins that regulate and contain microexons are involved in neurodevelopmental disorders. In the brains of individuals with autism spectrum disorder (ASD), the level of SRRM4 is reduced, leading to the misregulated splicing of multiple microexons (Irimia et al., 2014). Mice haploinsufficient for Srrm4 display reduced social interaction, sensory hypersensitivity, and impaired synaptic transmission (Quesnel-Vallières et al., 2015). Furthermore, Srrm4 is involved in regulating the ASD-relevant KCC2-dependent GABAergic excitatory to inhibitory switch (Nakano et al., 2019), and a mouse model of ASD with disrupted *Pten* has decreased Srrm4 expression and microexon inclusion (Thacker et al., 2020). Loss-of-function variants in its interacting partner SRSF11 have been implicated in ASD in humans (C Yuen et al., 2017). While the behavioral roles of only a few microexons have been studied in detail (Gonatopoulos-Pournatzis and Blencowe, 2020), the elimination of one from Eif4g1 altered synaptic plasticity and social behavior in mice (Gonatopoulos-Pournatzis et al., 2020). Many genes containing microexons also lead to neurodevelopmental disorders when mutated in humans. Examples include *CASK*-mediated microcephaly and cerebellar hypoplasia, *SPTAN1*-mediated childhood-onset epilepsy, and *MAPK8IP3*-mediated intellectual disability (Giacomini et al., 2021; Platzer et al., 2019; Syrbe et al., 2017). Taken together, this splicing program, the genes with microexons, and microexons themselves are important to proper neural development.

Although most microexons are unstudied, detailed structural and functional characterization of a small subset has revealed involvement in synapse development. The most well-studied are found in the receptor-type tyrosine phosphatase (e.g., *ptprf*) and teneurin (e.g., *tenm4*) gene families. Recognized in the 1990s (O'Grady et al., 1994; Pulido et al., 1995), two microexons in presynaptic PTPδ (*Ptprd*), PTPσ (*Ptprs*), and LAR (*Ptprf*) modulate *trans*-synaptic interfaces and determine selective interaction with postsynaptic partners (Y. Li et al., 2015; Lin et al., 2018; Park et al., 2020; Um et al., 2014; Yamagata et al., 2015; Yim et al., 2013). Similarly, differential inclusion of two conserved microexons in teneurins can modulate *trans*-synaptic homophilic or heterophilic interactions through splicing-dependent, large conformational changes (Berns et al., 2018; Gogou et al., 2024; Li et al., 2020). While studying these cell adhesion molecules has highlighted how microexons can trigger differential protein-protein interactions, little is known about the developmental consequences of these biochemical switches in other protein classes.

Identifying the neurobiological roles of many individual microexons is a challenge. A vertebrate model is necessary for these studies; although there is a similar splicing mechanism in *Drosophila melanogaster*, there is no overlap of the individual microexons (Torres-Mendez et al., 2021). Thus, we used larval zebrafish, a vertebrate that supports more high-throughput studies than mammalian models (Thyme et al., 2019), to assess the brain activity, brain structure, and behavior of zebrafish larvae mutant for 45 microexons (**Figure 1A**).

Results

A recently developed computational tool identified microexons that are differentially spliced

during mouse brain development and conserved in zebrafish (Parada et al., 2021). Based on the intersection of these two sets, 95 microexons fulfilled both parameters (**Table S1**). Of these 95 microexons, 44 exist in a canonical layout in the zebrafish genome, with a TGC and UC repeats

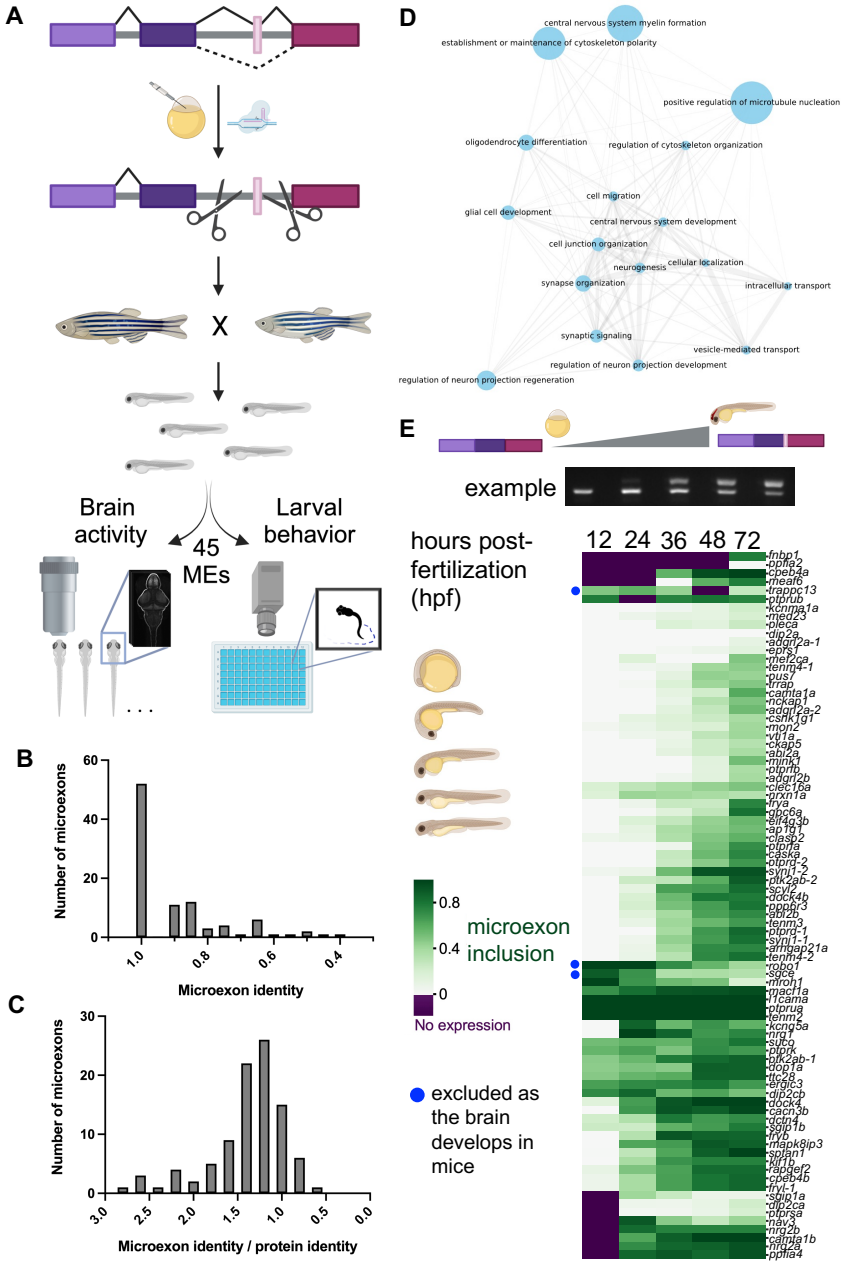

Fig. 1. Generation and analysis of zebrafish with mutations that remove conserved, developmentally regulated microexons. (**A**) Pipeline of the screen. Mutant lines with alternatively spliced microexons removed were generated with CRISPR/Cas9, crossed together, and sibling larvae were assessed for changes to brain morphology, brain activity, and behavioral profiling. Created with BioRender.com. (**B**) The amino acid sequence identity of 95 zebrafish microexons compared to mouse. (**C**) The amino acid sequence identity of 95 zebrafish microexons compared to mouse and divided by the sequence identity of the entire protein. (**D**) Gene Ontology analysis of biological processes associated with the 95 mouse microexons that are conserved in zebrafish. The analysis was completed using the PANTHER classification system. (**E**) Quantification of reverse transcription PCR (RT-PCR) for microexon-containing regions over zebrafish development. These data were clustered using the default seaborn clustermap settings (method = 'average').

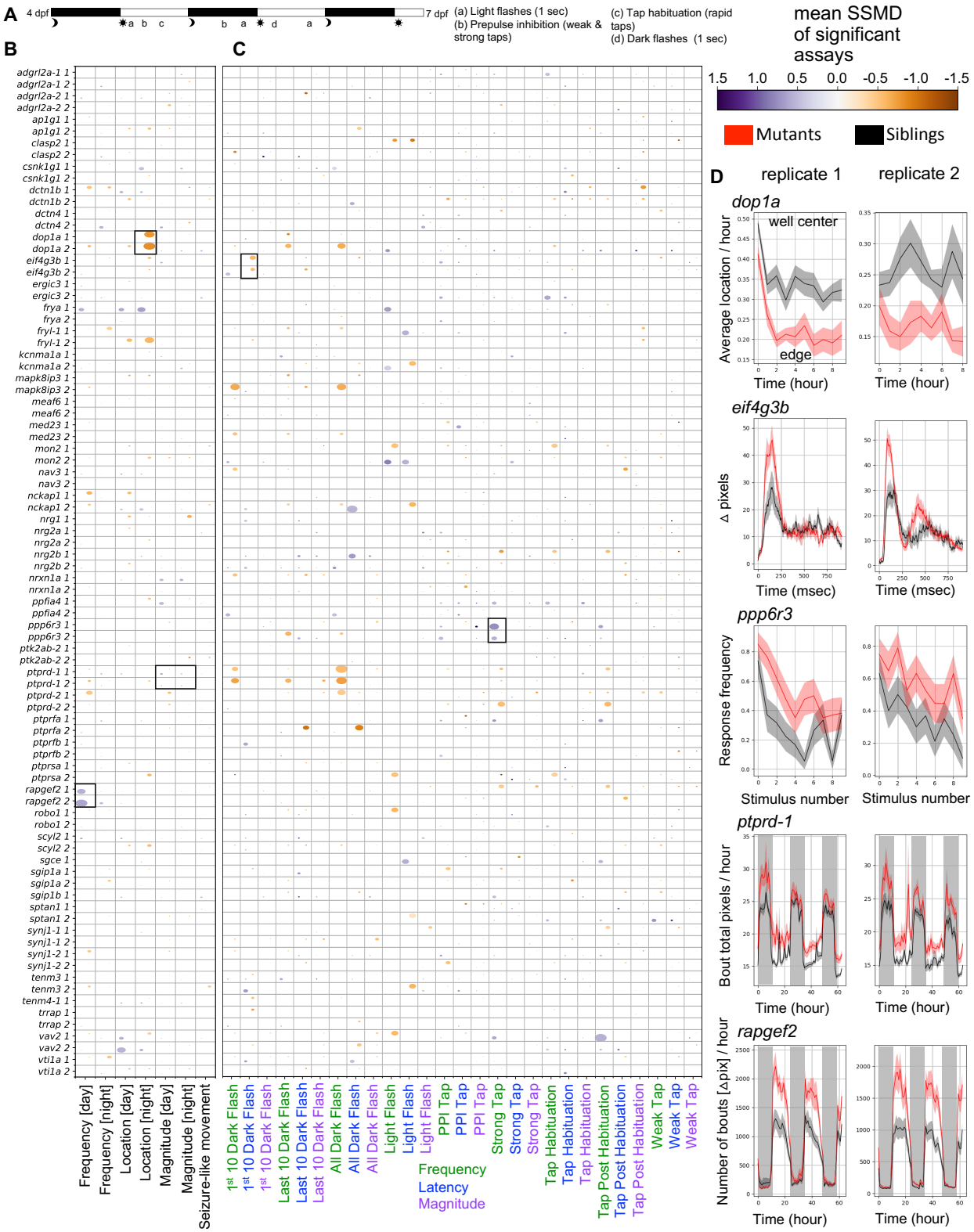

Fig. 2. Larval behavioral phenotypes of zebrafish with microexons removed. (**A**) Summary of behavioral pipeline. (**B**) Baseline behavioral phenotypes for microexon mutants. The labels "1" and "2" indicate biological replicates. The data shown is for homozygous mutant larvae compared to wild-type siblings. The size of the bubble represents the percent of significant measurements in the summarized category, and the color

represents the mean of the strictly standardized mean difference (SSMD) of the significant assays in that category. (**C**) Stimulus-driven behavioral phenotypes for microexon mutants. The labels "1" and "2" indicate biological replicates. The bubble size and color are calculated the same as in panel B. (**D**) Examples of behavioral phenotypes. The black boxes in panels B and C correspond to the selected plots. Wild-type siblings (black) are compared to the homozygous (red), and the plots show mean ± s.e.m.. All N are in Table S2. Kruskal-Wallis ANOVA p-values for the selected plots are as follows: *dop1a* center preference during the first night (day0night_boutcenterfraction_3600) = 0.00006/0.0008; *eif4g3b* p-values are not calculated for response plots (shown is all dark flashes in block 1), p-values for the latency for the first 10 dark flashes in block 1 (day6dpfdf1a_responselatency) = 0.026/0.0008,; *ppp6r3* frequency of response to strong acoustic stimuli with a sound frequency of 1000 hertz that precede the habituation block (day5dpfhab1pre_responsefrequency_1_a1f1000d5p) = 0.002/0.016; *ptprd*-1 pixels moved in each bout for the duration of the experiment (combo_boutcumulativemovement_3600) = 0.001/0.00002; *rapgef2* number of bouts for the duration of the experiment calculated using the delta pixel data in each frame (dpix_numberofbouts_3600) = 0.002/0.001.

directly upstream of the alternatively-spliced exon (Gonatopoulos-Pournatzis et al., 2018) (**Table S1**), indicating that their inclusion is likely controlled by Srrm4. Of the remaining microexons, most are similar to the canonical layout and are likely similarly regulated. The protein sequences of the 95 microexons are highly conserved between mouse and zebrafish (**Figure 1B**), more so than the full-length protein sequences (**Figure 1C**). The genes containing microexons are enriched for those involved in neuronal development as well as the cytoskeleton (**Figure 1D**). The majority of these microexons are included in transcripts as the brain develops, rather than lost, in both mouse and zebrafish (**Figure 1E**), making CRISPR/Cas9 removal of the microexon an ideal approach for studying the function of the added amino acids.

We generated 45 CRISPR/Cas9 lines that removed conserved microexons (Table S2) and assayed larval brain activity, brain structure, and behavior (**Figure 1A**). Protein-truncating mutations in additional genes that contain microexons revealed developmental and neural phenotypes in zebrafish (**Figure S1**, **Figure S2**), indicating the genes themselves are involved in biologically relevant pathways. Although we were most interested in those microexons only included after 24 hours post-fertilization (**Figure 1E**), we also removed microexons from several genes with an earlier expression of the isoform.

To uncover neural phenotypes, we assessed baseline and stimulus-driven movement. Homozygous mutant and control sibling larvae were subjected to a behavioral pipeline in 96-well plates from 4-7 days post-fertilization (dpf) (**Figure 2A**). Only a small number of strong, repeatable phenotypes were observed either at baseline or in response to acoustic or visual stimuli (**Figure 2B**, **Figure 2C**, **Figure S3**, **Figure S4**, **Figure S5**). Baseline behavioral differences were observed in multiple movement categories. For example, *rapgef2* mutants showed an increased movement frequency (**Figure 2B**, **Figure 2D**) but no changes to the characteristics of these movements (magnitude) or location in the well. In contrast, *dop1a* mutants had reduced daytime movement and an increased well-edge preference specifically at night (**Figure S4**, **Figure S6**, **Figure 2B**, **Figure 2D**). Other baseline movement phenotypes included a well-center preference for *vav2* mutants and a decreased movement magnitude for *ptprd*-2 (also referred to in the literature as meA) mutants (**Figure S6**). Dark-flash response phenotypes included a reduced latency for *eif4g3b* mutants and a reduced response frequency for *ptprd*-1 (meB) and *dop1a* mutants (**Figure 2C**, **Figure 2D**, **Figure S6**). Acoustic response phenotypes included an increased frequency of response to strong stimuli for *ppp6r3* mutants and a reduced frequency of response to strong acoustic stimuli for *ptprd*-2.

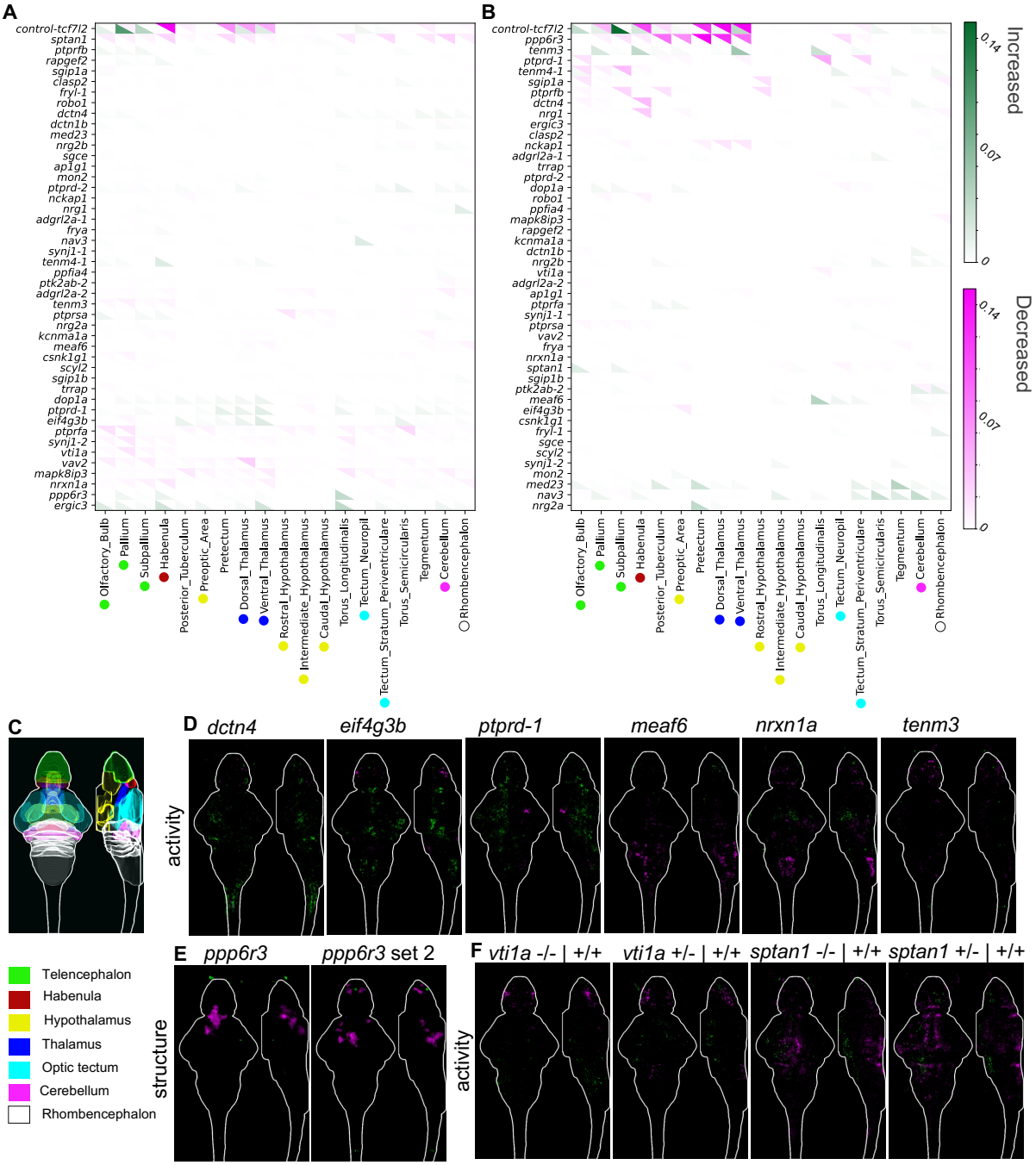

Fig. 3. Whole-brain activity and morphology phenotypes of zebrafish with microexons removed. (**A**) Summary of pErk comparisons between homozygous mutants and wild-type control siblings, where magenta represents decreased activity and green represents increased. The signal in each region was summed and divided by the region size. The N for all experiments is available in Table S2. (**B**) Summary of structure comparisons between homozygous mutants and wild-type control siblings, where magenta represents decreased size and green represents increased. (**C**) Location of major regions in the zebrafish brain based on masks from the Z-Brain atlas (Randlett et al., 2015). (**D**) Brain imaging for microexon mutants with repeatable brain activity phenotypes. The brain images represent the significant signal difference between homozygous and wild-type control siblings. They are shown as sum-of-slices projections (Z- and X- axes) with the white outline representing the zebrafish brain. (**E**) Structural phenotype of the *ppp6r3* mutant, with replicates shown side-by-side. The magenta indicates decreased size. (**F**) Brain imaging for two microexon mutants with brain activity phenotypes that are similar for both the heterozygous and homozygous mutants.

To detect changes to brain development and function, we collected phospho-Erk (pErk) brain activity maps under unstimulated conditions at 6 dpf. Large morphological differences were identified using the Jacobian matrix derived from the image registration process (Jefferis et al., 2007; Rohlfing and Maurer, 2003). Similar to the behavioral findings, few phenotypes were observed in brain activity (**Figure 3A**, **Figure S7**, **Figure S8**) or brain structure (**Figure 3B**, **Figure S9**, **Figure S10**) in homozygous mutants compared to wild-type control siblings when quantified by region (**Figure 3C**). Repeatable phenotypes were mild mild (**Figure 3D**) compared to a typical protein-truncating mutant (see control-*tcf7l2*). Only one mutant, *ppp6r3*, displayed substantial and repeatable differences in brain morphology (**Figure 3B**, **Figure 3E**), with reduced size observed mainly in the thalamus and neighboring pretectum. While the loss of both copies of microexons was required for most phenotypes, brain activity differences were observed in *vti1a* and *sptan1* heterozygotes (**Figure 3F**) as well as *vav2* and *mapk8ip3* (**Figure S7**, **Figure S8**).

Discussion

Our study provides a broad overview of the larval zebrafish neural phenotypes resulting from removing developmentally regulated microexons. Here, we leveraged our previously successful brain activity mapping and behavioral profiling strategy, which has high sensitivity and has uncovered phenotypes for dozens of mutants (Thyme et al., 2019). While only a few zebrafish lines had neural phenotypes, most removed microexons with behavioral or brain activity differences were completely unstudied previously and found in diverse protein classes.

The small number of observed phenotypes was unexpected based on conservation of the microexons (**Figure 1B**, **Figure 1C**) and the discovery rates of previous screens using similar methods (Capps et al., 2024; Thyme et al., 2019; Weinschutz Mendes et al., 2023). Although most of these studies focused on protein-truncating alleles, we have found phenotypes in lines with missense mutations (Capps et al., 2024). Furthermore, the genes that contain microexons are developmentally important (**Figure S1**). For instance, the *caska* loss-of-function mutant displayed substantial changes to brain activity, a smaller brain size, and multiple behavioral phenotypes. The low number and expressivity of microexon-specific phenotypes raises the question of whether perturbation of multiple microexons simultaneously, as was observed in the brains of autistic individuals (Irimia et al., 2014), would have a more pronounced effect. While zebrafish homozygous for *srrm4* deletion did not display any overt developmental phenotypes (Ciampi et al., 2022), a detailed neural characterization and behavior was not completed and this result is in contrast to a previous morpholino study (Calarco et al., 2009). Alternatively, although the microexons are present at larval stages, they may only become important during later stages of neuronal maturation that support more complex behaviors. Mouse models were studied as adults and for disruptions to social interaction, learning, and memory (Gonatopoulos-Pournatzis et al., 2020; Han et al., 2024), which larvae are not yet capable of (Dreosti et al., 2015; Valente et al., 2012).

Our study extends on findings for previously studied genes containing microexons. We discovered increased brain activity (**Figure 3D**) and an altered dark flash response in mutants for the *eif4g3b* (**Figure 4D**), whereas a mouse model with the microexon removed was described as having no behavior phenotypes (Gonatopoulos-Pournatzis et al., 2020). That study, however,

focused on social behavior, learning, and memory and may not have included stimuli analogous to dark flashes. Alternatively, microexon removal in zebrafish could have differential behavioral impacts than in rodents. Mice mutant for the *ptprd*-2 (meA) microexon have increased movement and interrupted sleep (Park et al., 2020). Both zebrafish mutants in *ptprd* demonstrate the opposite, with reduced daytime movement and increased sleep during the day for *ptprd*-2 (**Figure S6**). While the underlying disrupted circuitry could differ between the species, the daytime sleep increase raises the possibility of a rebound response to undetected disruptions to nighttime sleep. In other cases, the gene that contains the microexon has been extensively studied, but research on the microexon itself is absent. For example, the function of SNARE protein Vti1a in neural development and dense core vesicle biogenesis has been studied in great depth (Bollmann et al., 2022; Emperador-Melero et al., 2018; Kunwar et al., 2011; Sokpor et al., 2021; Walter et al., 2014). Its brain-specific microexon, however, was recognized over twenty years ago (Antonin et al., 2000), and its specific importance has been largely ignored. We discovered reduced brain activity mainly in the telencephalon in both homozygous and heterozygous lines (**Figure 3F**), highlighting the relevance of considering multiple conserved isoforms when characterizing protein function in the brain.

Mutants for unstudied microexons with the strongest phenotypes come from diverse protein classes (Gonatopoulos-Pournatzis and Blencowe, 2020), indicating this splicing program impacts neurodevelopmental processes beyond *trans*-synaptic partner selection. The only mutant with a substantial brain size difference was *ppp6r3*, which encodes a regulator of protein phosphatase 6 (PP6). Although little is known about this protein, it has been linked to cell cycle (Heo et al., 2020) and cell death (Wu et al., 2022), nominating hypotheses for determining future research on the source of the reduced size. Dctn4 is part of the dynactin complex, Mapk8ip3 is involved in Kinesin-1-Dependent axonal trafficking (Platzer et al., 2019; Watt et al., 2015), and Sptan1 is a cytoskeleton scaffold protein (Huang et al., 2017); the number microexon-containing genes related to the cytoskeleton (**Figure 1D**) and also trafficking (e.g., *vti1a*), suggests that microexons may be important to the unique cytoskeleton needs of developing neurons. The functions of microexons in cytoskeletal proteins are beginning to be discovered (Poliński et al., 2023). Transcriptional regulation is represented by the *meaf6* mutant, while Rapgef2, which has the strongest behavioral phenotypes upon microexon removal (**Figure 3D**), is a signaling protein. Although our list is not comprehensive, as many microexons remain unstudied, from 45 tested, we have prioritized approximately ten for future study. As microexons are often found in surface-accessible protein domains and can regulate protein-protein interactions (Dergai et al., 2010; Irimia et al., 2014), proximity-dependent ligation in zebrafish lines with and without the microexon could reveal differential binding partners *in vivo* (Rosenthal et al., 2021). The discovery of microexon mutants with neural phenotypes lays the groundwork for future investigation of impacted neurodevelopmental pathways and how interactomes differ between isoforms.

Materials and Methods

<u>Zebrafish husbandry</u>

The UAB Institutional Animal Care and Use Committee approved all zebrafish experiments (IACUC protocol numbers 22155 and 21744). Mutants were generated in an Ekkwill-based strain using CRISPR/Cas9 as previously described (Capps et al., 2024; Thyme et al., 2019)

(Table S2). Both adults and larvae were maintained on a 14 h/10 h light/dark cycle at 28°C. Experimental larvae were maintained at a density of less than 160 per dish in 150 mm petri dishes in fish water with methylene blue, and debris was removed at least twice prior to experimentation. Visibly unhealthy larvae and those without inflated swim bladders were excluded from experiments. Control animals were always siblings from the same clutch and derived from a single parental pair, and all larvae were genotyped after experimentation. The N for each assay is available in Table S2.

Brain activity and morphology

Phosphorylated-ERK (pErk) antibody staining was conducted as previously described (Capps et al., 2024; Thyme et al., 2019). The total ERK antibody (Cell Signaling, #4696) was used at 3:1000 and pErk antibody was used at 1:500 (Cell Signaling, #4370). Typically, the primary antibody exposure was for 2-3 days and secondary for one day. Image stacks were collected with a Zeiss LSM 900 upright confocal microscope using a 20X/1.0 NA water-dipping objective. These stacks were registered to the standard zebrafish Z-Brain reference using Computational Morphometry Toolkit (CMTK) (Jefferis et al., 2007; Randlett et al., 2015; Rohlfing and Maurer, 2003; Thyme et al., 2019). The significance threshold for MapMAPPING (Randlett et al., 2015; Thyme et al., 2019) was set based on a false discovery rate (FDR) where 0.05% of control pixels would be called as significant for both the brain activity and structural measurements.

Larval behavior

Larval behavior assays were conducted and analyzed as previously described (Capps et al., 2024; Joo et al., 2020; Thyme et al., 2019). The pipeline begins on the evening of larval stage 4 dpf and includes the following stimuli: 5 dpf light flashes (9:11-9:25), mixed acoustic stimuli (prepulse, strong, and weak, from 9:38-2:59), and three blocks of acoustic habituation (3:35-6:35); the night between 5 and 6 dpf mixed acoustic stimuli (1:02-5:00) and light flashes (6:01-6:20); 6 dpf three blocks of dark flashes with an hour between them (10:00-3:00) and mixed acoustic stimuli and light flashes (4:02-6:00). Stimulus responses were quantified from high-speed (285 frames-per-second) 1-second-long movies. All code for behavior analysis is available at https://github.com/thymelab/ZebrafishBehavior. Frequency of movement, magnitude of movement, and location preferences were calculated for the baseline data. An example of a "frequency" measure would be the active seconds / hour. An example of the "magnitude" measure would be the movement velocity of a bout. An example of a "location" measure would be the fraction of the bout time spent in the center of the well. Frequency, response magnitude parameters, and latency to response are also calculated for each stimulus response from the high-speed movies. The stimulus responses are also broken up into subsets, such as the dark flashes that occur at the beginning of the dark flash block and those that occur at the end. Multiple measures are calculated for the experiment, and both summarized and raw measures are shown in Figure 2 and the Supplementary Material. The summarized data is generated by merging related terms (e.g., all the "frequency" measures) together. The size of the bubble represents the percent of significant measurements in the summarized category, and the color represents the mean of the strictly standardized mean difference (SSMD) of the significant assays in that category. It is possible for some measures in the merged group to be increased (purple) and some decreased (orange), such as if a behavioral change occurs between 4 and 6 dpf, which is why it is possible to have two offset bubbles in each square. The scripts for merging these measurements

and generating the summarized bubble plot graphs are available at https://github.com/thymelab/DownstreamAnalysis.

Reverse Transcription PCR (RT-PCR)

RNA was extracted from zebrafish embryos using the E.Z.N.A. MicroElute Total RNA Kit (Omega Bio-Tek R6834-02), and cDNA synthesis was performed with iScript Reverse Transcription Supermix for RT-qPCR (Bio-Rad #1708840). Following PCR with GoTaq polymerase (Promega M7123) and primers (Table S1), samples were run on a 4% agarose gel and the band intensities were quantified using Fiji (Schindelin et al., 2012).

Data and materials availability

The mutants described in the paper are available from ZIRC. Code is available from https://github.com/thymelab. Processed behavioral and imaging data is available from Zenodo under the following DOIs: 10.5281/zenodo.13137486 (behavior output files), 10.5281/zenodo.13138646 (behavior input files), and 10.5281/zenodo.13138766 (brain activity mapping stacks).

Acknowledgments

This research was supported by a Mallinckrodt Award from the Edward Mallinckrodt Jr. Foundation (SBT). Guillermo Parada was instrumental to this work by sharing his list of conserved and developmentally regulated microexons while his study was still a preprint under review. We thank the UAB fish facility staff, the Zebrafish International Resource Center (ZIRC), particularly Andrzej Nasiadka, the Research Computing team at UAB, and the UAB Department of Neurobiology for supporting this study. We also thank the following Thyme lab members for experimental assistance or training that supported this study: Anna Moyer, Lynne Zhou, Vaishnavi Balaji, Alexia Barcus, and Sahil Malhotra.

Author contributions

SBT conceived of the study, analyzed imaging and behavioral data, and wrote the manuscript. VM, JW, and CLC generated the mutant lines. CCSC and KM initiated the project and CCSC collected most of the experimental data. MESC, WCG, MCK, CLC, and EGT contributed to the experimental data in this work by genotyping and propagating zebrafish lines, running larval behavior experiments, and collecting brain imaging data.

References

Antonin, W., Riedel, D., von Mollard, G.F., 2000. The SNARE Vti1a-beta is localized to small synaptic vesicles and participates in a novel SNARE complex. J. Neurosci. 20, 5724–5732. doi:10.1523/JNEUROSCI.20-15-05724.2000

Berns, D.S., DeNardo, L.A., Pederick, D.T., Luo, L., 2018. Teneurin-3 controls topographic circuit assembly in the hippocampus. Nature 554, 328–333. doi:10.1038/nature25463

Bollmann, C., Schöning, S., Kotschnew, K., Grosse, J., Heitzig, N., Fischer von Mollard, G., 2022. Primary neurons lacking the SNAREs vti1a and vti1b show altered neuronal development. Neural Dev. 17, 12. doi:10.1186/s13064-022-00168-2

Brugge, J.S., Cotton, P.C., Queral, A.E., Barrett, J.N., Nonner, D., Keane, R.W., 1985. Neurones express high levels of a structurally modified, activated form of pp60c-src. Nature 316, 554–557. doi:10.1038/316554a0

C Yuen, R.K., Merico, D., Bookman, M., L Howe, J., Thiruvahindrapuram, B., Patel, R.V., Whitney, J., Deflaux, N., Bingham, J., Wang, Z., Pellecchia, G., Buchanan, J.A., Walker, S., Marshall, C.R., Uddin, M., Zarrei, M., Deneault, E., D'Abate, L., Chan, A.J.S., Koyanagi, S., Paton, T., Pereira, S.L., Hoang, N., Engchuan, W., Higginbotham, E.J., Ho, K., Lamoureux, S., Li, W., MacDonald, J.R., Nalpathamkalam, T., Sung, W.W.L., Tsoi, F.J., Wei, J., Xu, L., Tasse, A.-M., Kirby, E., Van Etten, W., Twigger, S., Roberts, W., Drmic, I., Jilderda, S., Modi, B.M., Kellam, B., Szego, M., Cytrynbaum, C., Weksberg, R., Zwaigenbaum, L., Woodbury-Smith, M., Brian, J., Senman, L., Iaboni, A., Doyle-Thomas, K., Thompson, A., Chrysler, C., Leef, J., Savion-Lemieux, T., Smith, I.M., Liu, X., Nicolson, R., Seifer, V., Fedele, A., Cook, E.H., Dager, S., Estes, A., Gallagher, L., Malow, B.A., Parr, J.R., Spence, S.J., Vorstman, J., Frey, B.J., Robinson, J.T., Strug, L.J., Fernandez, B.A., Elsabbagh, M., Carter, M.T., Hallmayer, J., Knoppers, B.M., Anagnostou, E., Szatmari, P., Ring, R.H., Glazer, D., Pletcher, M.T., Scherer, S.W., 2017. Whole genome sequencing resource identifies 18 new candidate genes for autism spectrum disorder. Nat. Neurosci. 20, 602–611. doi:10.1038/nn.4524

Calarco, J.A., Superina, S., O'Hanlon, D., Gabut, M., Raj, B., Pan, Q., Skalska, U., Clarke, L., Gelinas, D., van der Kooy, D., Zhen, M., Ciruna, B., Blencowe, B.J., 2009. Regulation of vertebrate nervous system alternative splicing and development by an SR-related protein. Cell 138, 898–910. doi:10.1016/j.cell.2009.06.012

Capps, M.E.S., Moyer, A.J., Conklin, C.L., Martina, V., Torija-Olson, E.G., Klein, M.C., Gannaway, W.C., Calhoun, C.C.S., Vivian, M.D., Thyme, S.B., 2024. Diencephalic and Neuropeptidergic Dysfunction in Zebrafish with Autism Risk Mutations. BioRxiv. doi:10.1101/2024.01.18.576309

Ciampi, L., Mantica, F., López-Blanch, L., Permanyer, J., Rodriguez-Marín, C., Zang, J., Cianferoni, D., Jiménez-Delgado, S., Bonnal, S., Miravet-Verde, S., Ruprecht, V., Neuhauss, S.C.F., Banfi, S., Carrella, S., Serrano, L., Head, S.A., Irimia, M., 2022. Specialization of the photoreceptor transcriptome by Srrm3-dependent microexons is required for outer segment maintenance and vision. Proc. Natl. Acad. Sci. USA 119, e2117090119. doi:10.1073/pnas.2117090119

Dergai, M., Tsyba, L., Dergai, O., Zlatskii, I., Skrypkina, I., Kovalenko, V., Rynditch, A., 2010. Microexon-based regulation of ITSN1 and Src SH3 domains specificity relies on introduction of charged amino acids into the interaction interface. Biochem. Biophys. Res. Commun. 399, 307–312. doi:10.1016/j.bbrc.2010.07.080

Dreosti, E., Lopes, G., Kampff, A.R., Wilson, S.W., 2015. Development of social behavior in young zebrafish. Front. Neural Circuits 9, 39. doi:10.3389/fncir.2015.00039

Emperador-Melero, J., Huson, V., van Weering, J., Bollmann, C., Fischer von Mollard, G., Toonen, R.F., Verhage, M., 2018. Vti1a/b regulate synaptic vesicle and dense core vesicle secretion via protein sorting at the Golgi. Nat. Commun. 9, 3421. doi:10.1038/s41467-018-05699-z

Giacomini, T., Nuovo, S., Zanni, G., Mancardi, M.M., Cusmai, R., Pepi, C., Bertini, E., Valente, E.M., Battini, R., Ferrari, A., Romaniello, R., Zucca, C., Borgatti, R., Uccella, S., Severino, M., Striano, P., Pistorio, A., Prato, G., De Grandis, E., Nobili, L., Pisciotta, L., 2021. CASK related disorder: Epilepsy and developmental outcome. Eur J Paediatr

Neurol 31, 61–69. doi:10.1016/j.ejpn.2021.02.006
Gogou, C., Beugelink, J.W., Frias, C.P., Kresik, L., Jaroszynska, N., Drescher, U., Janssen, B.J.C., Hindges, R., Meijer, D.H., 2024. Alternative splicing controls teneurin-3 compact dimer formation for neuronal recognition. Nat. Commun. 15, 3648. doi:10.1038/s41467-024-47763-x
Gonatopoulos-Pournatzis, T., Blencowe, B.J., 2020. Microexons: at the nexus of nervous system development, behaviour and autism spectrum disorder. Curr. Opin. Genet. Dev. 65, 22–33. doi:10.1016/j.gde.2020.03.007
Gonatopoulos-Pournatzis, T., Niibori, R., Salter, E.W., Weatheritt, R.J., Tsang, B., Farhangmehr, S., Liang, X., Braunschweig, U., Roth, J., Zhang, S., Henderson, T., Sharma, E., Quesnel-Vallières, M., Permanyer, J., Maier, S., Georgiou, J., Irimia, M., Sonenberg, N., Forman-Kay, J.D., Gingras, A.-C., Collingridge, G.L., Woodin, M.A., Cordes, S.P., Blencowe, B.J., 2020. Autism-Misregulated eIF4G Microexons Control Synaptic Translation and Higher Order Cognitive Functions. Mol. Cell 77, 1176–1192.e16. doi:10.1016/j.molcel.2020.01.006
Gonatopoulos-Pournatzis, T., Wu, M., Braunschweig, U., Roth, J., Han, H., Best, A.J., Raj, B., Aregger, M., O'Hanlon, D., Ellis, J.D., Calarco, J.A., Moffat, J., Gingras, A.-C., Blencowe, B.J., 2018. Genome-wide CRISPR-Cas9 Interrogation of Splicing Networks Reveals a Mechanism for Recognition of Autism-Misregulated Neuronal Microexons. Mol. Cell 72, 510–524.e12. doi:10.1016/j.molcel.2018.10.008
Han, K.A., Yoon, T.-H., Kim, J., Lee, J., Lee, J.Y., Jang, G., Um, J.W., Kim, J.K., Ko, J., 2024. Specification of neural circuit architecture shaped by context-dependent patterned LAR-RPTP microexons. Nat. Commun. 15, 1624. doi:10.1038/s41467-024-45695-0
Heo, J., Larner, J.M., Brautigan, D.L., 2020. Protein kinase CK2 phosphorylation of SAPS3 subunit increases PP6 phosphatase activity with Aurora A kinase. Biochem. J. 477, 431–444. doi:10.1042/BCJ20190740
Huang, C.Y.-M., Zhang, C., Ho, T.S.-Y., Oses-Prieto, J., Burlingame, A.L., Lalonde, J., Noebels, J.L., Leterrier, C., Rasband, M.N., 2017. αii spectrin forms a periodic cytoskeleton at the axon initial segment and is required for nervous system function. J. Neurosci. 37, 11311–11322. doi:10.1523/JNEUROSCI.2112-17.2017
Irimia, M., Weatheritt, R.J., Ellis, J.D., Parikshak, N.N., Gonatopoulos-Pournatzis, T., Babor, M., Quesnel-Vallières, M., Tapial, J., Raj, B., O'Hanlon, D., Barrios-Rodiles, M., Sternberg, M.J.E., Cordes, S.P., Roth, F.P., Wrana, J.L., Geschwind, D.H., Blencowe, B.J., 2014. A highly conserved program of neuronal microexons is misregulated in autistic brains. Cell 159, 1511–1523. doi:10.1016/j.cell.2014.11.035
Jefferis, G.S.X.E., Potter, C.J., Chan, A.M., Marin, E.C., Rohlfing, T., Maurer, C.R., Luo, L., 2007. Comprehensive maps of Drosophila higher olfactory centers: spatially segregated fruit and pheromone representation. Cell 128, 1187–1203. doi:10.1016/j.cell.2007.01.040
Joo, W., Vivian, M.D., Graham, B.J., Soucy, E.R., Thyme, S.B., 2020. A Customizable Low-Cost System for Massively Parallel Zebrafish Behavioral Phenotyping. Front. Behav. Neurosci. 14, 606900. doi:10.3389/fnbeh.2020.606900
Kunwar, A.J., Rickmann, M., Backofen, B., Browski, S.M., Rosenbusch, J., Schöning, S., Fleischmann, T., Krieglstein, K., Fischer von Mollard, G., 2011. Lack of the endosomal SNAREs vti1a and vti1b led to significant impairments in neuronal development. Proc. Natl. Acad. Sci. USA 108, 2575–2580. doi:10.1073/pnas.1013891108
Li, J., Xie, Y., Cornelius, S., Jiang, X., Sando, R., Kordon, S.P., Pan, M., Leon, K., Südhof, T.C.,

Zhao, M., Araç, D., 2020. Alternative splicing controls teneurin-latrophilin interaction and synapse specificity by a shape-shifting mechanism. Nat. Commun. 11, 2140. doi:10.1038/s41467-020-16029-7

Li, Y., Zhang, P., Choi, T.-Y., Park, S.K., Park, H., Lee, E.-J., Lee, D., Roh, J.D., Mah, W., Kim, R., Kim, Y., Kwon, H., Bae, Y.C., Choi, S.-Y., Craig, A.M., Kim, E., 2015. Splicing-Dependent Trans-synaptic SALM3-LAR-RPTP Interactions Regulate Excitatory Synapse Development and Locomotion. Cell Rep. 12, 1618–1630. doi:10.1016/j.celrep.2015.08.002

Li, Y.I., Sanchez-Pulido, L., Haerty, W., Ponting, C.P., 2015. RBFOX and PTBP1 proteins regulate the alternative splicing of micro-exons in human brain transcripts. Genome Res. 25, 1–13. doi:10.1101/gr.181990.114

Lin, L., Zhang, M., Stoilov, P., Chen, L., Zheng, S., 2020. Developmental Attenuation of Neuronal Apoptosis by Neural-Specific Splicing of Bak1 Microexon. Neuron 107, 1180–1196.e8. doi:10.1016/j.neuron.2020.06.036

Lin, Z., Liu, J., Ding, H., Xu, F., Liu, H., 2018. Structural basis of SALM5-induced PTPδ dimerization for synaptic differentiation. Nat. Commun. 9, 268. doi:10.1038/s41467-017-02414-2

Martinez, R., Mathey-Prevot, B., Bernards, A., Baltimore, D., 1987. Neuronal pp60c-src contains a six-amino acid insertion relative to its non-neuronal counterpart. Science 237, 411–415. doi:10.1126/science.2440106

Nakano, Y., Wiechert, S., Bánfi, B., 2019. Overlapping Activities of Two Neuronal Splicing Factors Switch the GABA Effect from Excitatory to Inhibitory by Regulating REST. Cell Rep. 27, 860–871.e8. doi:10.1016/j.celrep.2019.03.072

O'Grady, P., Krueger, N.X., Streuli, M., Saito, H., 1994. Genomic organization of the human LAR protein tyrosine phosphatase gene and alternative splicing in the extracellular fibronectin type-III domains. J. Biol. Chem. 269, 25193–25199. doi:10.1016/S0021-9258(17)31516-8

Parada, G.E., Munita, R., Georgakopoulos-Soares, I., Fernandes, H.J.R., Kedlian, V.R., Metzakopian, E., Andres, M.E., Miska, E.A., Hemberg, M., 2021. MicroExonator enables systematic discovery and quantification of microexons across mouse embryonic development. Genome Biol. 22, 43. doi:10.1186/s13059-020-02246-2

Park, H., Choi, Y., Jung, H., Kim, S., Lee, S., Han, H., Kweon, H., Kang, S., Sim, W.S., Koopmans, F., Yang, E., Kim, H., Smit, A.B., Bae, Y.C., Kim, E., 2020. Splice-dependent trans-synaptic PTPδ-IL1RAPL1 interaction regulates synapse formation and non-REM sleep. EMBO J. 39, e104150. doi:10.15252/embj.2019104150

Platzer, K., Sticht, H., Edwards, S.L., Allen, W., Angione, K.M., Bonati, M.T., Brasington, C., Cho, M.T., Demmer, L.A., Falik-Zaccai, T., Gamble, C.N., Hellenbroich, Y., Iascone, M., Kok, F., Mahida, S., Mandel, H., Marquardt, T., McWalter, K., Panis, B., Pepler, A., Pinz, H., Ramos, L., Shinde, D.N., Smith-Hicks, C., Stegmann, A.P.A., Stöbe, P., Stumpel, C.T.R.M., Wilson, C., Lemke, J.R., Di Donato, N., Miller, K.G., Jamra, R., 2019. De Novo Variants in MAPK8IP3 Cause Intellectual Disability with Variable Brain Anomalies. Am. J. Hum. Genet. 104, 203–212. doi:10.1016/j.ajhg.2018.12.008

Poliński, P., Miret Cuesta, M., Zamora-Moratalla, A., Mantica, F., Cantero-Recasens, G., Normanno, D., Iñiguez, L.P., Morenilla-Palao, C., Ordoño, P., Bonnal, S., Ellis, J.D., Gómez Riera, R., De Lagrán Cabredo, M.M., Fernández-Blanco, Á., Rodríguez-Marin, C., Permanyer, J., Fölsz, O., Dominguez-Sala, E., Sierra, C., Legutko, D., Wojnacki, J.,

Musoles Lleo, J.L., Muñoz López, F.J., Blencowe, B.J., Herrera, E., Dierssen, M., Irimia, M., 2023. A highly conserved neuronal microexon in DAAM1 controls actin dynamics, RHOA/ROCK signaling, and memory formation. BioRxiv. doi:10.1101/2023.01.12.523772

Pulido, R., Serra-Pagès, C., Tang, M., Streuli, M., 1995. The LAR/PTP delta/PTP sigma subfamily of transmembrane protein-tyrosine-phosphatases: multiple human LAR, PTP delta, and PTP sigma isoforms are expressed in a tissue-specific manner and associate with the LAR-interacting protein LIP.1. Proc. Natl. Acad. Sci. USA 92, 11686–11690. doi:10.1073/pnas.92.25.11686

Quesnel-Vallières, M., Irimia, M., Cordes, S.P., Blencowe, B.J., 2015. Essential roles for the splicing regulator nSR100/SRRM4 during nervous system development. Genes Dev. 29, 746–759. doi:10.1101/gad.256115.114

Randlett, O., Wee, C.L., Naumann, E.A., Nnaemeka, O., Schoppik, D., Fitzgerald, J.E., Portugues, R., Lacoste, A.M.B., Riegler, C., Engert, F., Schier, A.F., 2015. Whole-brain activity mapping onto a zebrafish brain atlas. Nat. Methods 12, 1039–1046. doi:10.1038/nmeth.3581

Rohlfing, T., Maurer, C.R., 2003. Nonrigid image registration in shared-memory multiprocessor environments with application to brains, breasts, and bees. IEEE Trans. Inf. Technol. Biomed. 7, 16–25. doi:10.1109/titb.2003.808506

Rosenthal, S.M., Misra, T., Abdouni, H., Branon, T.C., Ting, A.Y., Scott, I.C., Gingras, A.-C., 2021. A toolbox for efficient proximity-dependent biotinylation in zebrafish embryos. BioRxiv. doi:10.1101/2021.05.16.444353

Schindelin, J., Arganda-Carreras, I., Frise, E., Kaynig, V., Longair, M., Pietzsch, T., Preibisch, S., Rueden, C., Saalfeld, S., Schmid, B., Tinevez, J.-Y., White, D.J., Hartenstein, V., Eliceiri, K., Tomancak, P., Cardona, A., 2012. Fiji: an open-source platform for biological-image analysis. Nat. Methods 9, 676–682. doi:10.1038/nmeth.2019

Sokpor, G., Rosenbusch, J., Kunwar, A.J., Rickmann, M., Tuoc, T., Rizzoli, S.O., Tarabykin, V., von Mollard, G.F., Krieglstein, K., Staiger, J.F., 2021. Ablation of Vti1a/1b Triggers Neural Progenitor Pool Depletion and Cortical Layer 5 Malformation in Late-embryonic Mouse Cortex. Neuroscience 463, 303–316. doi:10.1016/j.neuroscience.2021.03.021

Syrbe, S., Harms, F.L., Parrini, E., Montomoli, M., Mütze, U., Helbig, K.L., Polster, T., Albrecht, B., Bernbeck, U., van Binsbergen, E., Biskup, S., Burglen, L., Denecke, J., Heron, B., Heyne, H.O., Hoffmann, G.F., Hornemann, F., Matsushige, T., Matsuura, R., Kato, M., Korenke, G.C., Kuechler, A., Lämmer, C., Merkenschlager, A., Mignot, C., Ruf, S., Nakashima, M., Saitsu, H., Stamberger, H., Pisano, T., Tohyama, J., Weckhuysen, S., Werckx, W., Wickert, J., Mari, F., Verbeek, N.E., Møller, R.S., Koeleman, B., Matsumoto, N., Dobyns, W.B., Battaglia, D., Lemke, J.R., Kutsche, K., Guerrini, R., 2017. Delineating SPTAN1 associated phenotypes: from isolated epilepsy to encephalopathy with progressive brain atrophy. Brain 140, 2322–2336. doi:10.1093/brain/awx195

Thacker, S., Sefyi, M., Eng, C., 2020. Alternative splicing landscape of the neural transcriptome in a cytoplasmic-predominant Pten expression murine model of autism-like Behavior. Transl. Psychiatry 10, 380. doi:10.1038/s41398-020-01068-x

Thyme, S.B., Pieper, L.M., Li, E.H., Pandey, S., Wang, Y., Morris, N.S., Sha, C., Choi, J.W., Herrera, K.J., Soucy, E.R., Zimmerman, S., Randlett, O., Greenwood, J., McCarroll, S.A., Schier, A.F., 2019. Phenotypic Landscape of Schizophrenia-Associated Genes

Defines Candidates and Their Shared Functions. Cell 177, 478–491.e20. doi:10.1016/j.cell.2019.01.048

Torres-Mendez, A., Pop, S., Bonnal, S., Almudi, I., Roberts, R.J.V., Paolantoni, C., Alcaina, A., Avola, A., Martin Anduaga, A., Haussmann, I.H., Morin, V., Soller, M., Kadener, S., Roignant, J.-Y., Prieto-Godino, L., Irimia, M., 2021. Parallel evolution of a splicing program controlling neuronal excitability in flies and mammals. BioRxiv. doi:10.1101/2021.02.24.432780

Um, J.W., Kim, K.H., Park, B.S., Choi, Y., Kim, D., Kim, C.Y., Kim, S.J., Kim, M., Ko, J.S., Lee, S.-G., Choii, G., Nam, J., Heo, W.D., Kim, E., Lee, J.-O., Ko, J., Kim, H.M., 2014. Structural basis for LAR-RPTP/Slitrk complex-mediated synaptic adhesion. Nat. Commun. 5, 5423. doi:10.1038/ncomms6423

Valente, A., Huang, K.-H., Portugues, R., Engert, F., 2012. Ontogeny of classical and operant learning behaviors in zebrafish. Learn. Mem. 19, 170–177. doi:10.1101/lm.025668.112

Vuong, C.K., Black, D.L., Zheng, S., 2016. The neurogenetics of alternative splicing. Nat. Rev. Neurosci. 17, 265–281. doi:10.1038/nrn.2016.27

Walter, A.M., Kurps, J., de Wit, H., Schöning, S., Toft-Bertelsen, T.L., Lauks, J., Ziomkiewicz, I., Weiss, A.N., Schulz, A., Fischer von Mollard, G., Verhage, M., Sørensen, J.B., 2014. The SNARE protein vti1a functions in dense-core vesicle biogenesis. EMBO J. 33, 1681–1697. doi:10.15252/embj.201387549

Watt, D., Dixit, R., Cavalli, V., 2015. JIP3 Activates Kinesin-1 Motility to Promote Axon Elongation. J. Biol. Chem. 290, 15512–15525. doi:10.1074/jbc.M115.651885

Weinschutz Mendes, H., Neelakantan, U., Liu, Y., Fitzpatrick, S.E., Chen, T., Wu, W., Pruitt, A., Jin, D.S., Jamadagni, P., Carlson, M., Lacadie, C.M., Enriquez, K.D., Li, N., Zhao, D., Ijaz, S., Sakai, C., Szi, C., Rooney, B., Ghosh, M., Nwabudike, I., Gorodezky, A., Chowdhury, S., Zaheer, M., McLaughlin, S., Fernandez, J.M., Wu, J., Eilbott, J.A., Vander Wyk, B., Rihel, J., Papademetris, X., Wang, Z., Hoffman, E.J., 2023. High-throughput functional analysis of autism genes in zebrafish identifies convergence in dopaminergic and neuroimmune pathways. Cell Rep. 42, 112243. doi:10.1016/j.celrep.2023.112243

Wu, G., Li, D., Liang, W., Sun, W., Xie, X., Tong, Y., Shan, B., Zhang, M., Lu, X., Yuan, J., Li, Y., 2022. PP6 negatively modulates LUBAC-mediated M1-ubiquitination of RIPK1 and c-FLIPL to promote TNFα-mediated cell death. Cell Death Dis. 13, 773. doi:10.1038/s41419-022-05206-9

Yamagata, A., Sato, Y., Goto-Ito, S., Uemura, T., Maeda, A., Shiroshima, T., Yoshida, T., Fukai, S., 2015. Structure of Slitrk2-PTPδ complex reveals mechanisms for splicing-dependent trans-synaptic adhesion. Sci. Rep. 5, 9686. doi:10.1038/srep09686

Yim, Y.S., Kwon, Y., Nam, J., Yoon, H.I., Lee, K., Kim, D.G., Kim, E., Kim, C.H., Ko, J., 2013. Slitrks control excitatory and inhibitory synapse formation with LAR receptor protein tyrosine phosphatases. Proc. Natl. Acad. Sci. USA 110, 4057–4062. doi:10.1073/pnas.1209881110